Spin waves in metallic iron and nickel measured by soft x-ray resonant inelastic scattering

N. B. Brookes,[1,2] D. Betto,[1,*] K. Cao,[3] Yi Lu,[4] K. Kummer,[1] and F. Giustino[5,6,7]

[1]*ESRF, The European Synchrotron, 71 Avenue des Martyrs, 38043 Grenoble, France*
[2]*Diamond Light Source, Harwell Science and Innovation Campus, Didcot, Oxfordshire OX11 0DE, United Kingdom*
[3]*Daresbury Laboratory, Daresbury, Warrington WA4 4AD, United Kingdom*
[4]*Institute for Theoretical Physics, Heidelberg University, Philosophenweg 19, 69120 Heidelberg, Germany*
[5]*Department of Materials, University of Oxford, 16 Parks Road, Oxford OX1 3PH, United Kingdom*
[6]*Oden Institute for Computational Engineering and Sciences, The University of Texas at Austin, Austin, Texas 78712, USA*
[7]*Department of Physics, The University of Texas at Austin, Austin, Texas 78712, USA*

(Received 20 July 2019; revised 6 July 2020; accepted 23 July 2020; published 14 August 2020)

The spin-wave dispersions in iron and nickel along the [111] direction are determined using soft x-ray resonant inelastic x-ray scattering (RIXS). For iron, a 10-nm thin film was studied and, over the limited q range accessible, the peaks disperse as expected for a spin wave and in agreement with inelastic neutron scattering (INS) results. At the higher q values damping is observed with the peaks weakening and broadening. This damping is less pronounced than in the INS studies. The RIXS results are also compared with *ab initio* spin fluctuation calculations. The calculations slightly underestimate the energy dispersion and the damping is larger than in the measurement. Nevertheless, the agreement between the RIXS results, INS studies, and the theory is quite satisfactory. For the single crystal of nickel, the measured q dispersion flattens out rapidly and the peaks broaden. The strong damping effect is reproduced by the spin fluctuation calculations but the energy of the peaks is largely overestimated. Nevertheless, the flattening of the dispersion is not reproduced by the calculations and, although similar effects were observed in early INS experiments, they are not seen in more recent work. Possible reasons for this are discussed. These measurements show that using soft x-ray RIXS to study spin fluctuations in metallic systems, which are in general very challenging for the technique, has much promise. More interestingly, since the iron measurements were performed on a 10-nm thin film, the study opens the possibility to study tailor-made thin-film samples, which cannot be easily studied by other techniques. Combining these studies with state-of-the-art *ab initio* calculations opens up interesting prospects for testing our understanding of spin waves in metallic systems.

DOI: 10.1103/PhysRevB.102.064412

I. INTRODUCTION

Despite studies of spin fluctuations in magnetic materials over many decades their importance is still current today. Spin fluctuations have been invoked in the mechanism of high-temperature superconductivity [1,2] and have importance for new applications as represented by fields like spintronics [3] and magnonics [4]. In addition, although much progress has been made [5–8], spin-wave theory still has problems in reproducing experimental results exactly (e.g., [9,10]).

The method of reference for studying magnetic excitations is often inelastic neutron scattering (INS). However, due to significant improvements in instrumentation for soft x-ray resonant inelastic scattering (RIXS) [11,12], in recent years, it has been shown that the technique has much potential for studying magnetic excitations in addition to low-energy electronic, lattice, and orbital excitations (see for example [13–17]). This is particularly due to improvements in energy resolution as well as the extension to studying three-dimensional (3D) reciprocal space [18]. Consequently, as the applicability of soft x-ray RIXS is being explored, it is natural to compare new data with existing INS results.

Many of the high-energy resolution RIXS studies so far have been on ionic materials like the transition metal oxides or poor metals like the doped iron and copper based superconductors, e.g., [19,20]. Little work has been done on pure metals [21,22] and none, to the authors' knowledge, with high-energy resolution sufficient to observe spin-wave dispersions. One reason is that the fluorescence yield can dominate the spectra making it difficult to determine low-energy losses.

In this paper we show that it is possible to use soft x-ray RIXS to study spin waves in the archetypical transition metals, iron and nickel. The results are compared with INS studies [23–36]. The energy dispersion, peak widths, and intensities show the interaction with the Stoner continuum [37] and the resulting Landau damping [37,38]. This is more evident in nickel than iron. The results for iron are in good agreement with INS results, whereas the nickel results are reminiscent of early INS results but do not agree very well with more recent INS data. The same can be said of the comparison for iron and nickel with spin-wave calculations [7,9,39–42]. On the theory

*Present address: Max Planck Institute for Solid State Research, Heisenbergstraße 1, 70569 Stuttgart, Germany.

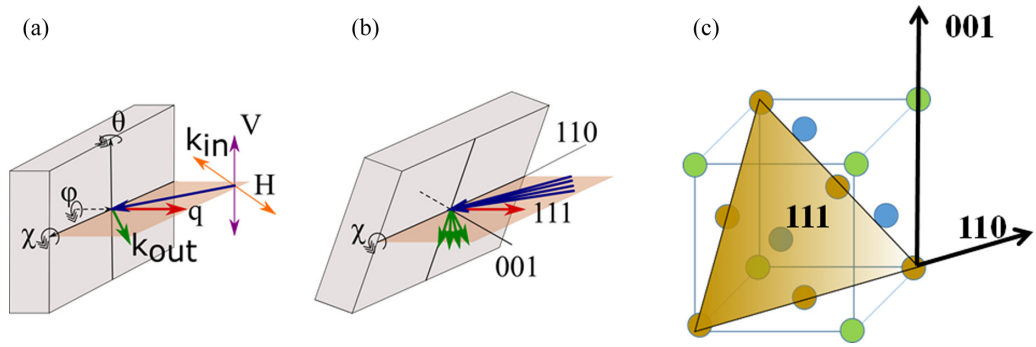

FIG. 1. (a) Generic RIXS measurement geometry, showing the rotation angles θ, ϕ, and χ. (b) Measurement geometry for the [111] dispersion, after rotation of the sample around χ. (c) The unit cell for fcc nickel showing the 111 plane.

side, time-dependent density functional perturbation theory (TDDFPT) has been shown to be a powerful tool to study spin fluctuations, by treating magnons and Stoner excitations on the same footing, thus capable of capturing Laudau damping. The method has been used to study spin fluctuations of pure metals and shown general agreement with INS data [5–9]. The current results are compared with these state-of-the-art calculations. Nevertheless, they show that there is still some discrepancy between measurements and theory, particularly for nickel. In addition, this work shows that surface science prepared samples can be studied using RIXS. In the case of nickel, a bulk Ni(001) sample was used and in the case of iron, a 10-nm-thick Fe(001) film grown on Ag(001). Both samples were prepared and transferred under ultrahigh vacuum (UHV) to the RIXS spectrometer. Consequently, these results expand the possibilities represented by this relatively new technique.

II. EXPERIMENTAL DETAILS

The high-energy resolution RIXS measurements were carried out at the ID32 beamline of the ESRF [12]. The photon energy was tuned to the L_3 absorption edge of Fe (∼707 eV) and 1 eV above the L_3 edge of Ni (∼853 eV). The energy resolution was set to ∼45 meV and the experiment took advantage of the three-circle high-precision goniometer and variable angle scattering arm [12] to allow the [111] high-symmetry direction to be followed in each case. Similar experiments on NiO have previously shown this capability [18].

The samples were prepared in the ID32 surface preparation facility [43]. The Ni(001) crystal was cleaned by repeated Ar^+ ion sputtering (1 keV and then 500 eV) at 800 K followed by annealing at the same temperature. The surface structure was checked using LEED. Once clean the sample was transferred to the RIXS chamber using a home-built UHV vacuum suitcase. The pressure rose briefly into the 10^{-7} mbar range while transferring. The measuring sample chamber pressure was $\sim 2\times10^{-9}$ mbar. The 10-nm Fe(001) film was grown on a Ag(001) single crystal that was cleaned by repeated Ar^+ (500 eV) sputtering cycles at ∼750 K followed by annealing at the same temperature. The surface structure was checked using LEED. The iron was evaporated from an *e*-beam evaporator and the flux calibrated using a water-cooled crystal monitor mounted at the sample position. The flux rate was controlled using an integrated evaporator flux monitor once the rate was established with the crystal monitor. The 10-nm film took approximately 30 min to grow and the chamber base pressure remained in the 10^{-10} mbar range. The substrate was kept at 300 K during the evaporation. The surface structure was checked using low-energy electron diffraction (LEED) and the pattern was as expected for Fe (001) [44]. The sample was transferred to the RIXS chamber using a commercial UHV vacuum suitcase (Ferrovac) which kept the pressure in the 10^{-10} mbar range. The RIXS transfer chamber was in the 10^{-8} mbar range and the sample chamber was in the low 10^{-9} mbar range.

The crystal was orientated with the [110] direction in the horizontal plane. Since the sample goniometer only allows a +/− 45° in the χ direction the samples were mounted on a 20° wedge. This allowed the sample to be rotated to 54.7° from the vertical direction to permit θ-2θ scans, so that the q along the [111] direction is probed. This requires the sample and scattering arm to be moved together. This procedure has been successfully used before in Ref. [18]. The scattering was in the horizontal plane. The incoming light polarization for the measurements was horizontal, i.e., in the scattering plane. The sample geometry is shown in Fig. 1. The measurements were made at 20 K. The samples were checked for cleanliness using total electron yield (TEY) x-ray-absorption spectroscopy (XAS) (see for example the XAS spectra in Figs. 2 and 3). The spectra were as expected for clean metals [45]. The samples were routinely checked with XAS during the measurements. The TEY XAS is much more surface sensitive than the RIXS measurement and is therefore a sensitive test of the sample surface state. Over long periods (hours) some contamination was observed in the XAS spectra but only where the beam was incident. To be sure that a clean part of the sample was always measured the samples were moved periodically. This was easily achieved since the x-ray beam spot size was $\sim 40\,\mu\text{m}\times 3.5\,\mu\text{m}$ [full width at half maximum (FWHM)] and the sample size $>4\times4\,\text{mm}^2$. The instrumental function was determined by measuring a strong specular signal at the measurement energy. The energy zero could also be calibrated in the same way.

Computational method

Calculations of the full response matrix has been performed using time-dependent density functional perturbation

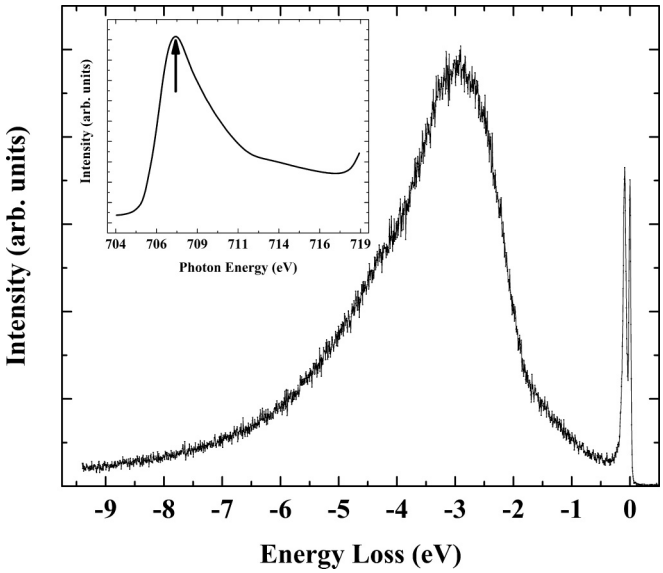

FIG. 2. Wide energy scan RIXS spectra from iron. The inset shows the iron XAS spectra and the arrow marks the energy used to take the RIXS spectra.

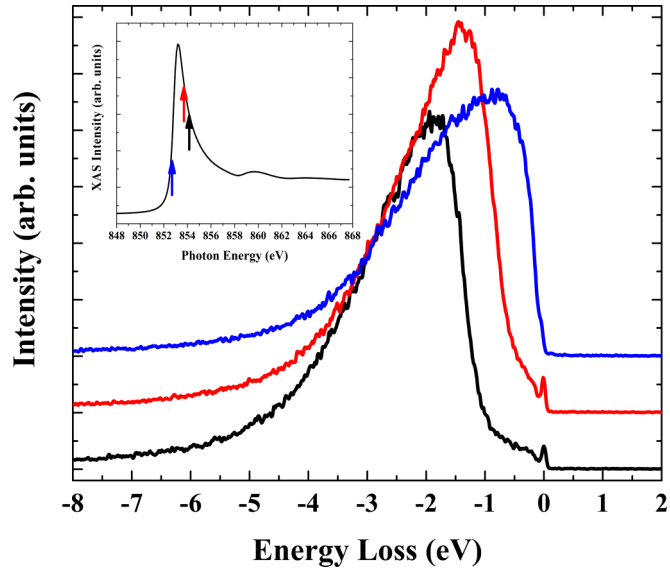

FIG. 3. Wide energy scan RIXS spectra from nickel. The inset shows the nickel XAS spectra and the arrows mark the energies used to take the RIXS spectra.

theory implemented on top of Quantum ESPRESSO [9,46]. An adiabatic local spin-density approximation and norm conserving pseudopotentials with a plane-wave kinetic-energy cutoff of ∼60 Ry were used. A 40×40×40 k-point mesh was employed for both ground-state and spin susceptibility calculations. A full description of the method could be found in Ref. [9]. The full response matrix can be written as $\chi^{ij}(q,\omega)$ $(i,j=0,x,y,z)$, where 0 denotes charge degree of freedom and x, y, z denote magnetization directions. The ground-state magnetization is by default along the z direction thus charge and z correspond to longitudinal components; x and y correspond to transverse components. Spin-orbit coupling is not considered and hence there is no cross-coupling between longitudinal and transverse directions. The number of terms are further reduced, due to the cubic symmetry, leaving $\chi^{xx}(q,\omega)$, $\chi^{xy}(q,\omega)$, $\chi^{zz}(q,\omega)$, and $\chi^{00}(q,\omega)$. $\chi^{00}(q,\omega)$ is in fact the dynamical dielectric response. The imaginary part of the transverse spin susceptibility, $\chi^{+-}(q,\omega)=\chi^{xx}-i\chi^{xy}$, contains the information of magnon excitations and is comparable to INS data.

III. RESULTS AND DISCUSSION

Figure 2 shows the wide energy window RIXS scan for iron ($q=0.692\,\text{Å}^{-1}$). The inset shows the L_3 absorption edge spectra characteristic of the metallic state [45]. There is a very strong fluorescence peak in the −1 to −7 eV energy-loss region, peaking at −3 eV with a tail that extends to zero energy loss. Nevertheless, there is a clear low-energy-loss peak just below the zero energy elastic peak, which is even slightly more intense than the elastic peak.

Figure 3 shows several wide energy window RIXS scans for nickel ($q=0.787\,\text{Å}^{-1}$) together with the L_3 absorption edge spectra. The different RIXS spectra are taken at the positions shown by the arrows in the figure inset. The fluorescence peak is much stronger and closer in energy to the elastic peak than in iron. If the energy is detuned −0.5 eV below the resonance the elastic peak is masked by the tail of the fluorescence. By going just above the resonance the fluorescence can be moved far enough away to be able to investigate the low-energy-loss region below the elastic peak. In the present study the photon energy was detuned to +1 eV above the edge (black curve in Fig. 3).

A. Iron RIXS

Figure 4 shows the q dependent RIXS energy-loss spectra in the first 300 meV. A clear separated peak is seen at high q which disperses towards the elastic peak at low q. The elastic peak is very strong at low scattering angles (small q). Nevertheless, the elastic peak shape and width is known from the reference measurements. Consequently, the elastic peak can be reliably fitted and the magnon peak position and shape extracted as shown in Fig. 4(c). The peak fitting results shown in Figs. 4(b) and 4(c) include a background resulting from the fluorescence, a resolution limited Gaussian elastic peak, and a loss peak. The loss feature was fitted with a symmetric peak shape (using an asymmetric peak as used below for nickel gave the same result).

The resulting peak position, intensity, and deconvoluted width (FWHM) for the loss features are shown in Fig. 5. The results from one of the neutron studies [28] are also shown as open triangles. The uncertainties in the RIXS energy position (black squares) are less than the symbol size. The neutron data are for a Fe(4%Si) sample but this gives similar results to pure Fe [24]. The agreement between the RIXS and INS data [28] is quite reasonable. The dashed line shows the theoretical spin-wave energy $E=Dq^2$ [32,37]. D is the spin-wave stiffness constant [37], with $D=230\,\text{meV Å}^2$, as found in more recent work from Fe(12%Si) [35]. A value of $D=260\,\text{meV Å}^2$ is found in Ref. [28]. The inset in Fig. 4 shows the spin-wave peak intensity which slowly

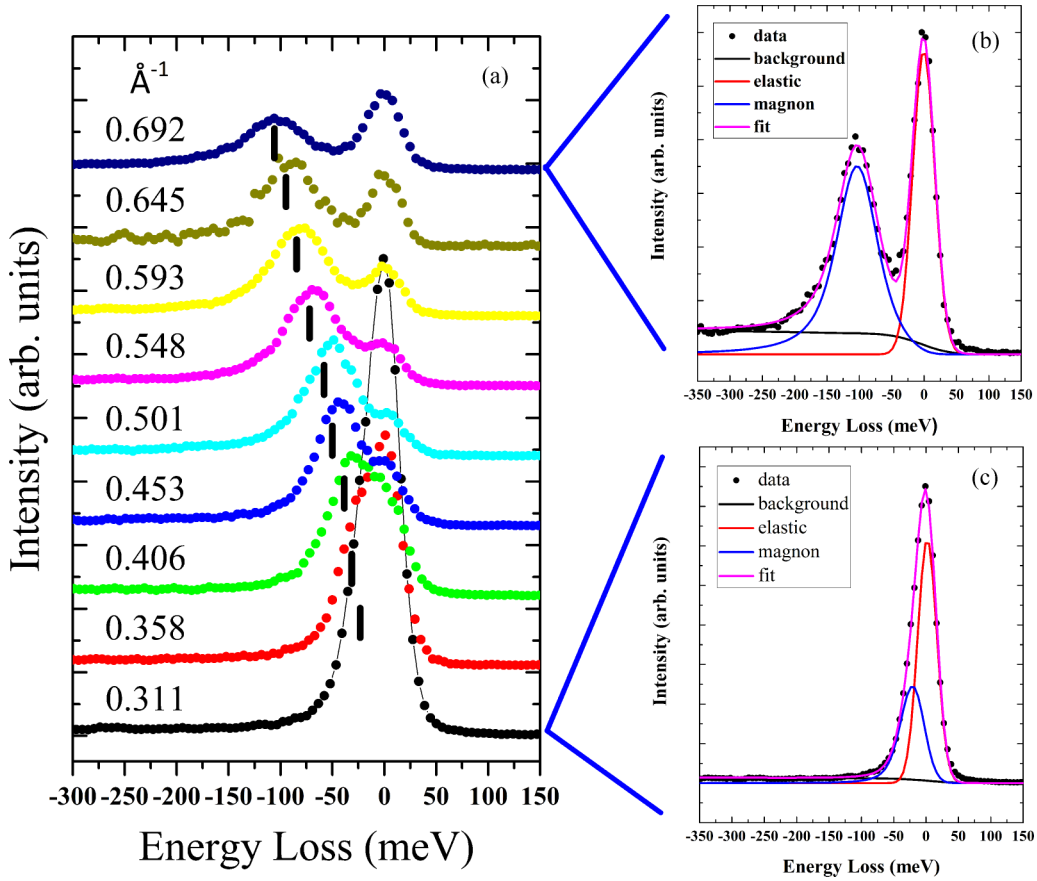

FIG. 4. (a) q-dependent RIXS spectra along the [111] direction in iron. The vertical bars mark the peak position found by peak fitting. (b) Peak fitting for $q = 0.692$ Å^{-1} and (c) for $q = 0.311$ Å^{-1}.

decreases with increasing q. At higher energy loss (∼80 meV, $q \geqslant 0.6$ Å^{-1}) the peak intensity starts to drop faster. In addition, the peak width doubles over the total measured q range.

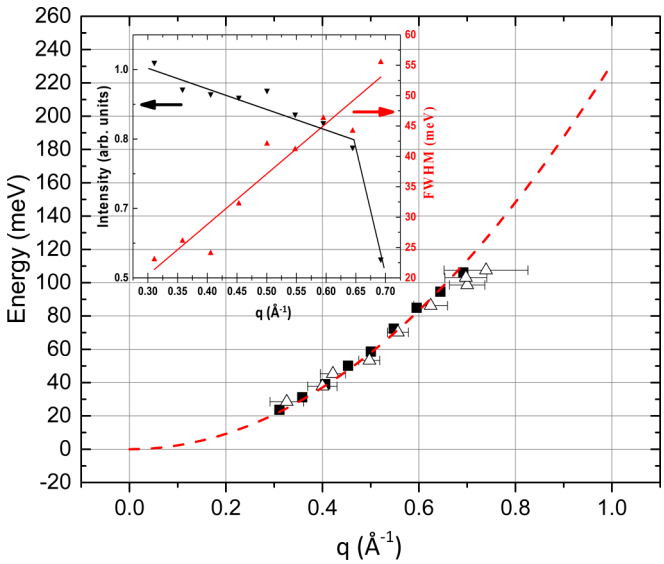

FIG. 5. Spin-wave dispersion for iron along the [111] direction. RIXS data (black squares), INS [28] open triangles. The dashed line is a parabolic curve with a stiffness constant $D = 230$ meV Å^2; see text. Inset: Intensity and deconvoluted width of the loss peaks.

Some of the previous INS data showed a dramatic drop in intensity over the same q range by a factor of ∼10 [28,35]. However, in the work of Loong *et al.* [32] reasonable intensity was measured out to energy losses of 160 meV along the [110] direction, similar to what is observed here. Loong *et al.* [32] used a very high purity single crystal of iron and also an instrument with higher sensitivity compared to earlier work [28]. However, in the RIXS data the peak intensity drops off faster than the increase in the peak width at higher q. This is probably due to the intensity starting to be spread out into a long weak tail, which cannot be distinguished easily in the experiment due to the fluorescent background, so that the intensity drop is overestimated. Such a tail is observed in the calculations as is shown below.

Figure 6 shows the results of the transverse spin susceptibility calculations in a color contour map. Profile cuts are shown for several q values in the right-hand panel. The RIXS data are plotted as black squares. In the RIXS experiment the spin-wave dispersion is slightly larger (as also seen in the INS data) than in the calculation. In addition, although experimentally a broadening and weakening of the peaks are observed (see Fig. 4), they are less noticeable than in the calculations. This is mostly because the calculated peaks at low q are much sharper than observed in the experiment. Nevertheless, if the area under the theoretical curves is compared at the various q values there is only a small decrease in intensity with increasing q. This is not so different from

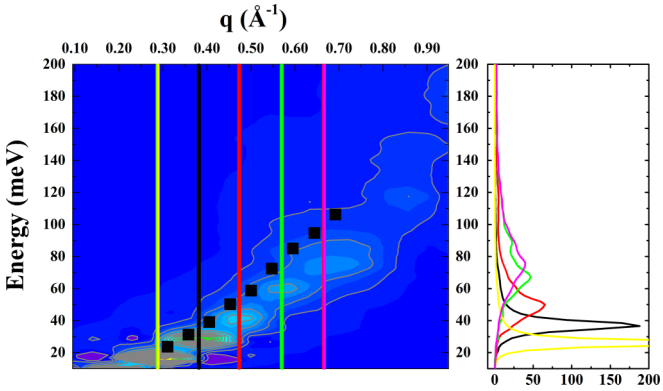

FIG. 6. Calculated $\mathrm{Im}\chi^{+-}(q,\omega)$ for iron along the [111] direction. The experimental results are shown as black squares. The right-hand panel shows cuts corresponding to the vertical lines in the left-hand panel.

what is seen in the experiment. Since the INS measurements give a variety of results for the peak intensities and widths and also show a different behavior from both the theory and the RIXS measurements it is difficult to make a comparison. We have also compared the RIXS results with all components of the response matrix and only find a correspondence with the transverse spin susceptibility response, consistent with the measurement of a spin-wave dispersion (see Appendix A).

B. Nickel RIXS

Figure 7 shows the q-dependent RIXS energy-loss spectra in the first 300 meV. At higher q a separated peak can be seen. The exact determination of the peak positions is much more difficult than in iron due to the high background and weaker signal. In order to determine the peak positions, the spectra were fitted with a background coming from the fluorescence peak and an energy resolution limited elastic peak. The latter can be determined by measuring below the resonance energy, at a q value with no loss peaks, or by using a reference sample close to the measured nickel sample. This also allows the energy zero to be determined. Several different functions were investigated to represent the fluorescence background. These included a simple linear fit, a polynomial fit as used previously [19], and the background shown which is a modification of that used in Ref. [19] and similar to that in Ref. [47]. We find that the final peak position and shape is little affected by the choice of background function. The elastic peak and background were subtracted from the spectra to leave the magnetic peaks. The resulting peaks have an asymmetric shape, where the asymmetry increases with q. These peaks were fitted with a "Fano" line shape [48]. Examples of the fitting are shown in Figs. 7(b) and 7(c).

The resulting peak position, intensity, and deconvoluted width (FWHM) for the loss features are shown in Fig. 8 (black squares). The results from two neutron studies are also

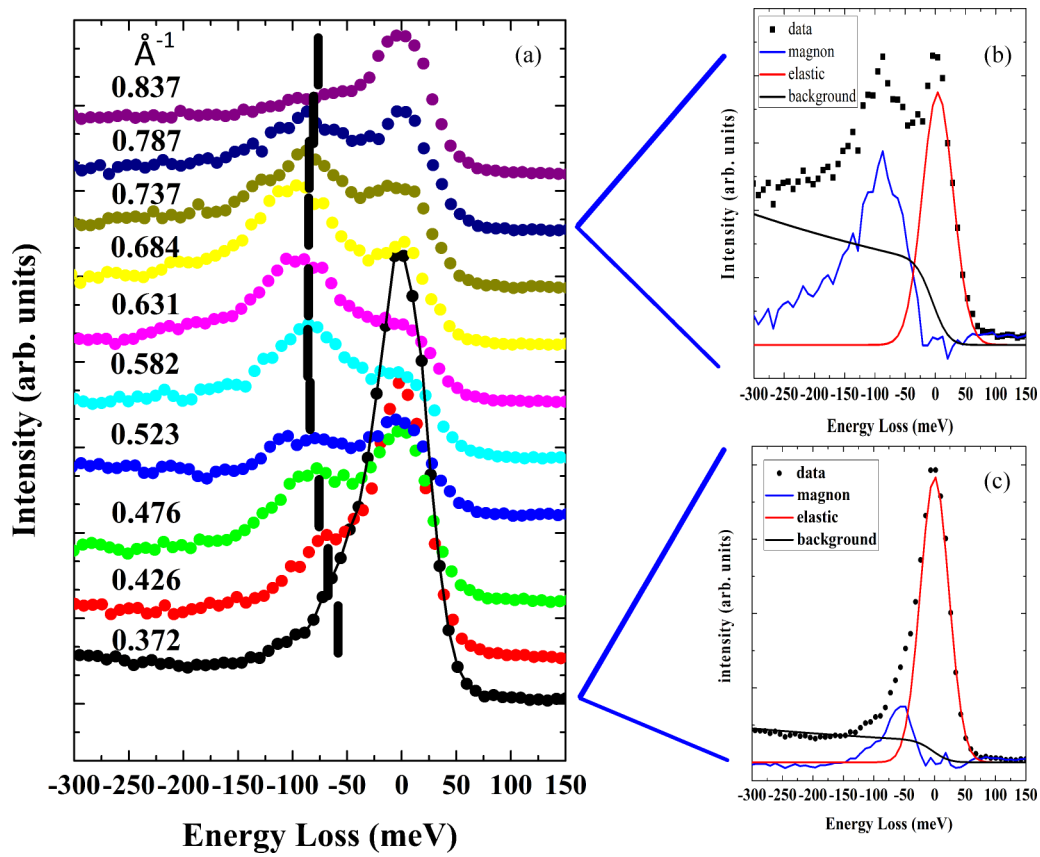

FIG. 7. (a) q-dependent RIXS spectra along the [111] direction in nickel. The vertical bars mark the peak position found by peak fitting. (b) Peak fitting for $q = 0.787$ Å^{-1} and (c) for $q = 0.372$ Å^{-1}.

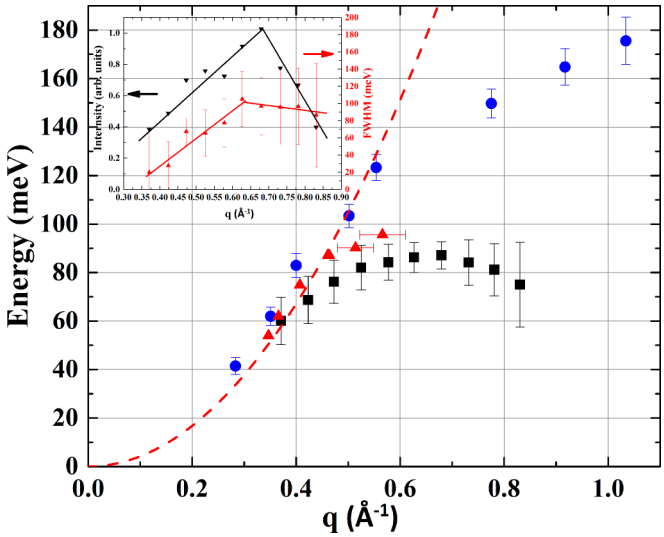

FIG. 8. Spin-wave dispersion for nickel along the [111] direction. RIXS data (black squares), INS data (triangles [30] and dots [33]). The dashed line represents a spin-wave curve with $D = 433$ meV Å^2. Inset: Peak intensity and width of the loss peaks.

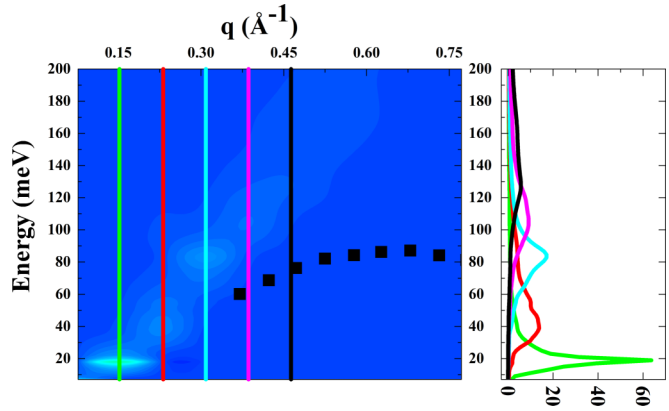

FIG. 9. Calculated $\mathrm{Im}\chi^{+-}(q,\omega)$ for nickel along the [111] direction. The experimental results are shown as black squares. The right-hand panel shows two cuts given by the vertical lines in the left-hand panel.

shown as triangles [30] and dots [33]. The agreement between the RIXS and INS data is consistent over the first few data points but the RIXS data rapidly flatten out from $q \geqslant 0.5$ Å^{-1} similarly to the data of Refs. [26,30] but contrary to Ref. [33]. The difference between the various neutron experiments was explained as being due to using an instrument with improved sensitivity and also to having a very high purity nickel crystal. This reduced the incoherent scattering and contributions from phonon scattering. This possibly indicates that, also in the case of RIXS measurements, the crystal quality may influence the results. This is important for future work and for the use of thin films, which can be studied using RIXS. The inset of Fig. 8 shows the intensity dropping as the dispersion flattens; the peak width also increases from low to high q. As for iron, INS data show a large drop in intensity (around a factor of 10) at around 80 meV ($q \geqslant 0.65$ Å^{-1}). In the RIXS data this is a factor of 2. The dashed line is a spin-wave fit with $D = 433$ meV Å^2 [26] but without the data points at low q it is difficult to make a comparison with the RIXS data.

Figure 9 shows the results of the calculations in a color contour map. Profile cuts are shown for several q values in the right-hand panel. The RIXS data are shown as black squares. In the experiment the dispersion rapidly flattens out in the measured q range. The experimental values are at lower energy than the calculated ones. As seen in Fig. 8 the experimental data broaden and the intensity starts to decrease rapidly for the last few points. The cuts from the calculation shown in Fig. 9 also show a weakening and broadening of the spin waves but the energy scales for the calculations and experiment do not match exactly. Additionally, the damping is so strong that above $q = 0.45$ Å^{-1} it is difficult to identify a real peak corresponding to the spin wave. In the case of iron the calculated dispersion was slightly less than in the experiment. For nickel the calculated dispersion is larger and there is a broadening of the peaks but no flattening of the dispersion. The observed nickel peak dispersion discrepancy is similar to what was reported in Ref. [9], and is attributed to the overestimation of the Stoner splitting by the adiabatic local spin-density approximation to DFT.

The flattening and broadening of the spin waves has been associated with the interaction with the Stoner continuum of excitations. The Stoner spin gap energy is much lower in nickel than in iron explaining why the iron data are less affected in this q range, whereas the nickel data are strongly affected. The asymmetric line shape seen for nickel is probably a sign of the interaction with the Stoner continuum as is the much weaker peak intensity. The different results from various INS experiments also seem to indicate that sample quality and experimental sensitivity strongly affect the q range in which the peaks can be followed. In addition, we have investigated if the flattening of the dispersion might be due to measuring something other than the spin waves. As for iron above, we have also extended the DFT calculations to determine all the components of the response matrix in order to see if anything else corresponds to that observed in the experiment. We do not find anything in the calculations, which corresponds to the experimental data where it deviates from the spin-wave behavior (see Appendix A). Also, since RIXS is a relatively new technique and the measurement of magnetic excitations is not as well understood as in INS, one has to consider if this might be the origin of the differences. Although the two techniques do not measure exactly the same thing, RIXS captures qualitatively the magnon dispersion [49–51]. However, the other terms in the RIXS spectrum could contribute to some moderate uncertainties in determining the magnon energy [52,53]. Experimentally, previous work for example on the cuprates [54] and the present results for iron give very similar energy positions for the peaks found in INS and RIXS experiments. Nevertheless, to help understand the differences between the current experiments for nickel, we have used the QUANTY code [55] to calculate the RIXS cross section for Ni(111). This approach is certainly approximate, and not ideal, but gives an idea of the expected cross section. Assuming that the single-crystal sample has multiple (111) domains (the most likely case), then the averaged RIXS cross section over the experimentally observed parameter space does not vary

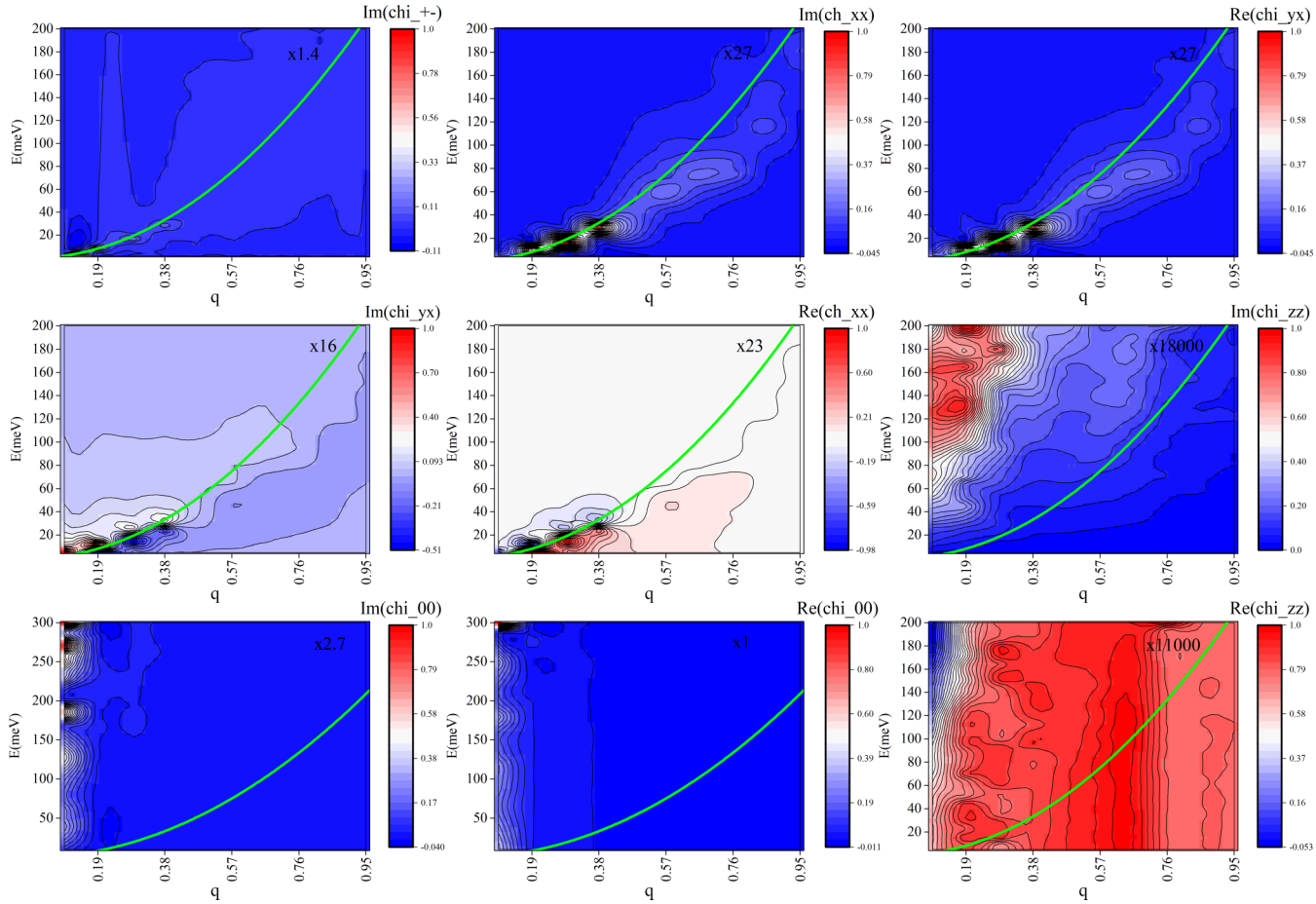

FIG. 10. Calculated Re and Im parts of $\chi^{xx}(q,\omega)$, $\chi^{xy}(q,\omega)$, $\chi^{zz}(q,\omega)$, $\chi^{00}(q,\omega)$ functions for Fe(111). The top-left panel shows the spin fluctuations given by $\mathrm{Im}\chi^{+-}(q,\omega)$. The color scale is on a linear scale but each panel has been scaled to 1. The multiplication factor is given in each panel. The green line gives the spin-wave fit derived from this and previous work.

significantly (see Appendix B). One interesting point is that for some specific magnetic domains the RIXS cross section is much reduced in the q range where we measured (see Appendix B). Although this would explain a reduced intensity, it does not explain the flattening of the dispersion. It nevertheless points to the importance of carrying out experiments on single domain thin films in the future and to taking into account the geometrical effect on the RIXS cross section. Overall, we still do not have a very good understanding of the nickel data and as with the early INS experiments there is a need for further experiments, particularly on thin films where the sample quality and domain structure can be controlled better.

IV. CONCLUSION AND FUTURE PROSPECTS

This study shows that it is in principle possible to measure spin waves in purely metallic systems using soft x-ray RIXS, even considering all the technical difficulties. The restricted q range in soft x-ray RIXS is an unavoidable problem but measurements at even lower q should be possible with newer instruments if the elastic peak does not dominate the spectra. This work opens the way to the study of various metallic systems in thin-film form or in heterostructures, for example CoFe in spin valves or tunnel junctions. In addition, new phases could be studied, e.g., bcc nickel or bcc cobalt. In principle, studies could also go down to the monolayer level provided there is sufficient signal. One could also think of looking at the effect of strain by an appropriate choice of substrate. In addition, the temperature dependence of the spin waves and their damping could be investigated. Clearly much work has and will be done with inelastic neutron scattering, which is the benchmark technique, and it is gratifying to see reasonable agreement in these soft x-ray RIXS measurements and INS experiments. This work will hopefully stimulate ideas for new complementary experiments that can be done with soft x-ray RIXS.

Finally, it should be said that the theoretical approach used here shows much promise in calculating the spin fluctuations in these basic magnetic materials [9]. Improvements in the way the exchange-correlation potential is treated should improve agreement. Further neutron and x-ray experiments should be able to help develop these computational methods to a point where they become predictive tools. In addition, there is a great need for full RIXS calculations, taking into account all the process influencing the cross section, including the spectroscopic factors and the fundamental properties of the material being probed.

ACKNOWLEDGMENTS

N.B.B. would like to thank A. Boothroyd, T. Perring, and K. Gilmore for useful discussions and Diamond Light Source for hosting him during the period of time this paper was written.

APPENDIX A

The results of the calculations for the full response matrix as described in the main text and Ref. [9] are shown for iron and nickel in Figs. 10 and 11 respectively. The q range covers that measured in the experiment. The green lines show the spin-wave fit to the experimental data as a guide for the eye.

APPENDIX B

The RIXS cross section for all possible (111) magnetic domains have been calculated for a Ni crystal using the QUANTY code [53], following the approach used in Ref. [49] but adapted to a ferromagnetic arrangement of spins. In this approach, a low-energy effective RIXS scattering operator is used to calculated the transition probabilities, which are then mapped out into reciprocal space using linearized spin-wave theory [56]. The parameters for the Ni atoms have been calculated using Cowan's code [57] and some crystal-field energy has been added in order to stabilize a single magnetic ground state. The calculations have been performed with crossed incoming and outgoing light polarizations. While these calculations are not well suited for metallic samples due to the high electronic screening and the delocalized nature of the excitations, we believe that they can nevertheless provide the qualitative behavior of the spin-wave excitations measured with RIXS for simple ferromagnetic or antiferromagnetic arrangements of spins. The intensity of the magnons are shown as log color maps for each domain together with the average over all domains in Fig. 12. In some domains the intensity is reduced in the middle of the zone as a result of the scattering geometry and the spins direction. The experimental values fall between the two vertical lines in the middle panel. For the [1 −1 1] and [1 −1 −1] domains the intensity drops by 25 times going to higher q. For the average over all domains the intensity varies +/− 50% in the experimental q interval.

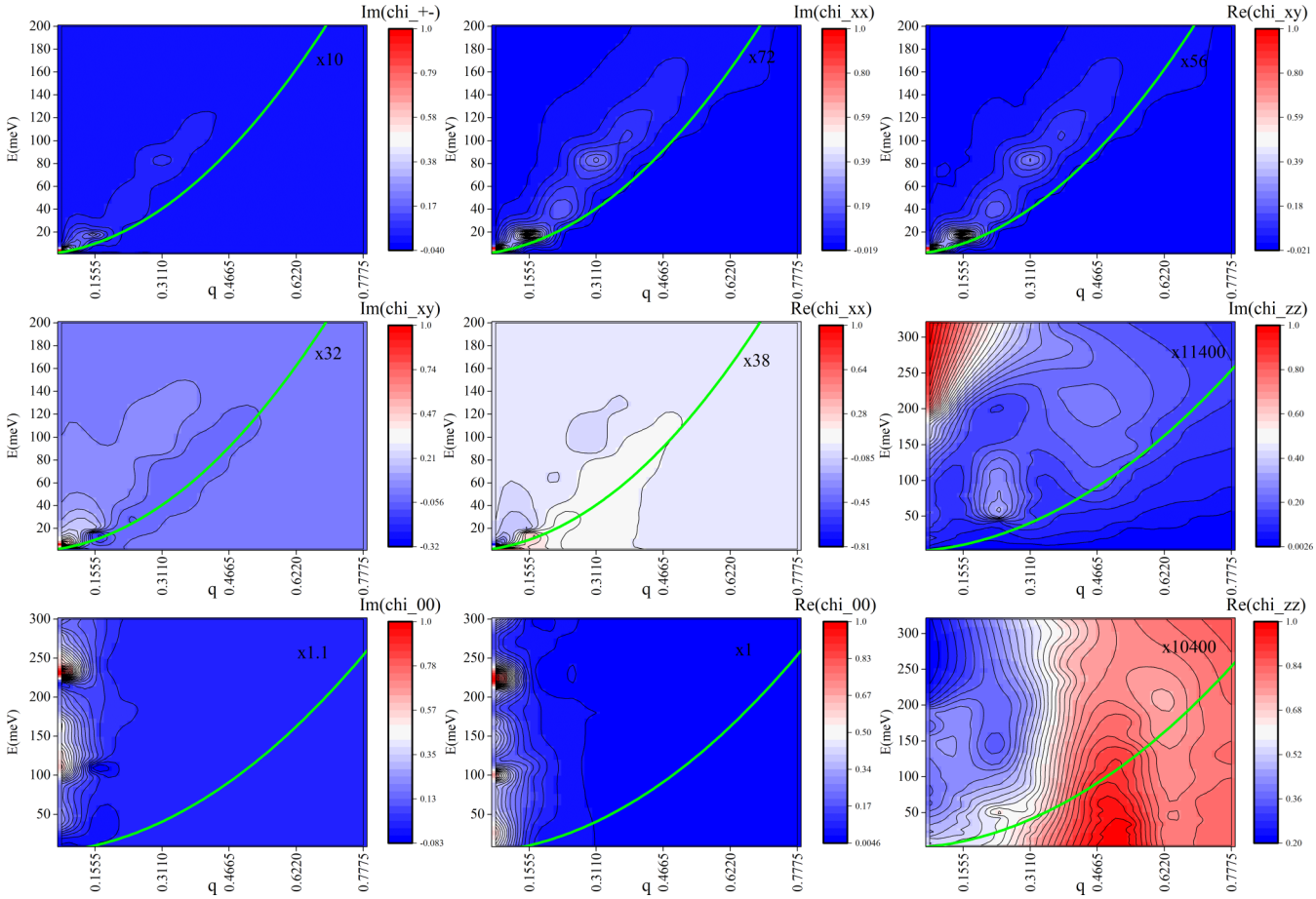

FIG. 11. Calculated Re and Im parts of $\chi^{xx}(q,\omega)$, $\chi^{xy}(q,\omega)$, $\chi^{zz}(q,\omega)$, $\chi^{00}(q,\omega)$ functions for Ni(111). The top-left panel shows the spin fluctuations given by $\mathrm{Im}\chi^{+-}(q,\omega)$. The color scale is on a linear scale but each panel has been scaled to 1. The multiplication factor is given in each panel. The green line gives the spin-wave fit derived from this and previous work.

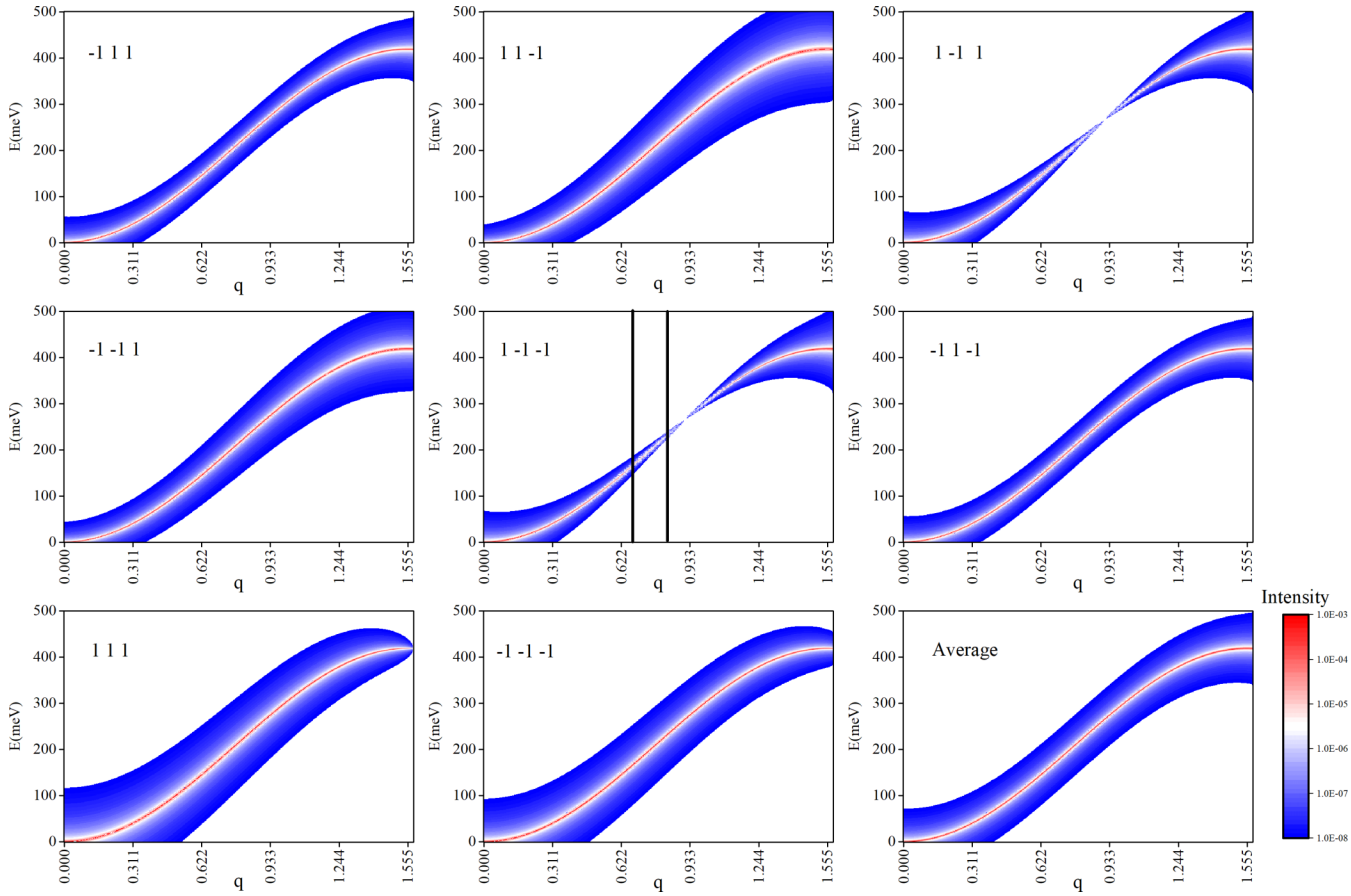

FIG. 12. The calculation of the RIXS cross section for the 8 [111] magnetic domains and their average for Ni(111). The scale bar shows the intensity of five decades on a log scale. The center panel shows one of the examples where the cross section is reduced in the center of the zone. The q region measured in the experiment is marked by the two vertical lines. The q scale is in Å^{-1}.

[1] D. J. Scalapino, Rev. Mod. Phys. **84**, 1383 (2012).

[2] B. Keimer, S. A. Kivelson, M. R. Norman, S. Uchida, and J. Zaanen, Nature (London) **518**, 179 (2015).

[3] S. A. Wolf, D. D. Awschalom, R. A. Buhrman, J. M. Daughton, S. von Molnár, M. L. Roukes, A. Y. Chtchelkanova, and D. M. Treger, Science **294**, 1488 (2001).

[4] V. V. Kruglyak, S. O. Demokritov, and D. Grundler, J. Phys. D: Appl. Phys. **43**, 264001 (2010).

[5] P. Buczek, A. Ernst, and L. M. Sandratskii, Phys. Rev. B **84**, 174418 (2011).

[6] S. Y. Savrasov, Phys. Rev. Lett. **81**, 2570 (1998).

[7] B. Rousseau, A. Eiguren, and A. Bergara, Phys. Rev. B **85**, 054305 (2012).

[8] T. Gorni, I. Timrov, and S. Baroni, Eur. Phys. J. B **91**, 249 (2018).

[9] K. Cao, H. Lambert, P. G. Radaelli, and F. Giustino, Phys. Rev. B **97**, 024420 (2018).

[10] V. P. Antropov, B. N. Harmon, and A. N. Smirnov, J. Magn. Magn. Mater. **200**, 148 (1999).

[11] G. Ghiringhelli, A. Piazzalunga, C. Dallera, G. Trezzi, L. Braicovich, T. Schmitt, V. N. Strocov, R. Betemps, L. Patthey, X. Wang, and M. Grioni, Rev. Sci. Instrum. **77**, 113108 (2006).

[12] N. B. Brookes, F. Yakhou-Harris, K. Kummer, A. Fondacaro, J. C. Cezar, D. Betto, E. Velez-Fort, A. Amorese, G. Ghiringhelli, L. Braicovich, R. Barrett, G. Berruyer, F. Cianciosi, L. Eybert, P. Marion, P. van der Linden, and L. Zhang, Nucl. Instrum. Methods Phys. Res. A **903**, 175 (2018).

[13] G. Ghiringhelli, M. Le Tacon, M. Minola, S. Blanco-Canosa, C. Mazzoli, N. B. Brookes, G. M. De Luca, A. Frano, D. G. Hawthorn, F. He, T. Loew, M. M. Sala, D. C. Peets, M. Salluzzo, E. Schierle, R. Sutarto, G. A. Sawatzky, E. Weschke, B. Keimer, and L. Braicovich, Science **337**, 821 (2012).

[14] H. Miao, J. Lorenzana, G. Seibold, Y. Y. Peng, A. Amorese, F. Yakhou-Harris, K. Kummer, N. B. Brookes, R. M. Konik, V. Thampy, G. D. Gu, G. Ghiringhelli, L. Braicovich, and M. P. M. Dean, Proc. Natl. Acad. Sci. USA **114**, 12430 (2017).

[15] L. Chaix, G. Ghiringhelli, Y. Y. Peng, M. Hashimoto, B. Moritz, K. Kummer, N. B. Brookes, Y. He, S. Chen, S. Ishida, Y. Yoshida, H. Eisaki, M. Salluzzo, L. Braicovich, Z.-X. Shen, T. P. Devereaux, and W.-S. Lee, Nat. Phys. **13**, 952 (2017).

[16] Y. Y. Peng, G. Dellea, M. Minola, M. Conni, A. Amorese, D. Di Castro, G. M. De Luca, K. Kummer, M. Salluzzo, X. Sun, X. J. Zhou, G. Balestrino, M. Le Tacon, B. Keimer, L. Braicovich, N. B. Brookes, and G. Ghiringhelli, Nat. Phys. **13**, 1201 (2017).

[17] M. Hepting, L. Chaix, E. W. Huang, R. Fumagalli, Y. Y. Peng, B. Moritz, K. Kummer, N. B. Brookes, W. C. Lee, M. Hashimoto, T. Sarkar, J.-F. He, C. R. Rotundu, Y. S. Lee,

R. L. Greene, L. Braicovich, G. Ghiringhelli, Z. X. Shen, T. P. Devereaux, and W. S. Lee, Nature (London) **563**, 374 (2018).
[18] D. Betto, Y. Y. Peng, S. B. Porter, G. Berti, A. Calloni, G. Ghiringhelli, and N. B. Brookes, Phys. Rev. B **96**, 020409(R) (2017).
[19] K. Zhou, Y. Huang, C. Monney, X. Dai, V. N Strocov, N. Wang, Z.-G. Chen, C. Zhang, P. Dai, L. Patthey, J. van den Brink, H. Ding, and T. Schmitt, Nat. Commun. **4**, 1470 (2013).
[20] L. J. P. Ament, M. van Veenendaal, T. P. Devereaux, J. P. Hill, and J. van den Brink, Rev. Mod. Phys. **83**, 705 (2011).
[21] C. F. Hague, J.-M. Mariot, P. Strange, P. J. Durham, and B. L. Gyorffy, Phys. Rev. B **48**, 3560(R) (1993).
[22] L.-C. Duda, J. Stöhr, D. C. Mancini, A. Nilsson, N. Wassdahl, J. Nordgren, and M. G. Samant, Phys. Rev. B **50**, 16758(R) (1994).
[23] G. Shirane, R. Nathans, O. Steinsvoll, H. A. Alperin, and S. J. Pickart, Phys. Rev. Lett. **15**, 146 (1965).
[24] G. Shirane, V. J. Minkiewicz, and R. Nathans, J. Appl. Phys. **39**, 383 (1968).
[25] V. J. Minkiewicz, M. F. Collins, R. Nathans, and G. Shirane, Phys. Rev. **182**, 624 (1969).
[26] H. A. Mook, R. M. Nicklow, E. D. Thompson, and M. K. Wilkinson, J. Appl. Phys. **40**, 1450 (1969).
[27] E. D. Thompson and H. A. Mook, J. Appl. Phys. **41**, 1227 (1970).
[28] H. A. Mook and R. M. Nicklow, J. Phys. Colloq. **32**, C1-1177 (1971).
[29] H. A. Mook and R. M. Nicklow, Phys. Rev. B **7**, 336 (1973).
[30] H. A. Mook and D. Tocchetti, Phys. Rev. Lett. **43**, 2029 (1979).
[31] J. W. Lynn and H. A. Mook, Phys. Rev. B **23**, 198 (1981).
[32] C.-K. Loong, J. M. Carpenter, J. W. Lynn, R. A. Robinson, and H. A. Mook, J. Appl. Phys. **55**, 1895 (1984).
[33] H. A. Mook and D. Mck. Paul, Phys. Rev. Lett. **54**, 227 (1985).
[34] J. F. Cooke, J. A. Blackman, and T. Morgan, Phys. Rev. Lett. **54**, 718 (1985).
[35] M. Yethiraj, R. A. Robinson, D. S. Sivia, J. W. Lynn, and H. A. Mook, Phys. Rev. B **43**, 2565 (1991).
[36] T. G. Perring, A. T. Boothroyd, D. Mck. Paul, A. D. Taylor, R. Osborn, R. J. Newport, J. A. Blackman, and H. A. Mook, J. Appl. Phys. **69**, 6219 (1991).
[37] N. B. Melnikov and B. I. Reser, *Dynamic Spin-Fluctuation Theory of Metallic Magnetism* (Springer, Cham, 2018).
[38] A. T. Costa, R. B. Muniz, and D. L. Mills, Phys. Rev. B **68**, 224435 (2003).
[39] T. Izuyama, D.-J. Kim, and R. Kubo, J. Phys. Soc. Jpn. **18**, 1025 (1963).
[40] M. Pajda, J. Kudrnovský, I. Turek, V. Drchal, and P. Bruno, Phys. Rev. B **64**, 174402 (2001).
[41] E. Şaşıoğlu, A. Schindlmayr, C. Friedrich, F. Freimuth, and S. Blügel, Phys. Rev. B **81**, 054434 (2010).
[42] X. Wu, Z. Liu, and T. Luo, J. Appl. Phys. **123**, 085109 (2018).
[43] K. Kummer, A. Fondacaro, E. Jimenez, E. Velez-Fort, A. Amorese, M. Aspbury, F. Yakhou-Harris, P. van der Linden, and N. B. Brookes, J. Synchrotron Radiat. **23**, 464 (2016).
[44] F. Ciccacci, G. Chiaia, and S. De Rossi, Solid State Commun. **88**, 827 (1993).
[45] J. Stohr and R. Nakajima, IBM J. Res. Dev. **42**, 73 (1998).
[46] P. Giannozzi, O. Andreussi, T. Brumme, O. Bunau, M. Nardelli, M. Calandra, R. Car, C. Cavazzoni, D. Ceresoli, M. Cococcioni, N. Colonna, I. Carnimeo, A. Dal Corso, S. de Gironcoli, P. Delugas, R. A. DiStasio, A. Ferretti, A. Floris, G. Fratesi, G. Fugallo *et al.*, J. Phys.: Condens. Matter **29**, 465901 (2017).
[47] H. C. Robarts, M. Barthélemy, K. Kummer, M. Garcia-Fernández, J. Li, A. Nag, A. C. Walters, K. J. Zhou, and S. M. Hayden, Phys. Rev. B **100**, 214510 (2019).
[48] U. Fano, Phys. Rev. **124**, 1866 (1961).
[49] M. W. Haverkort, Phys. Rev. Lett. **105**, 167404 (2010).
[50] C. J. Jia, E. A. Nowadnick, K. Wohlfeld, Y. F. Kung, C.-C. Chen, S. Johnston, T. Tohyama, B. Moritz, and T. P. Devereaux, Nat. Commun. **5**, 3314 (2014).
[51] C. Jia, K. Wohlfeld, Y. Wang, B. Moritz, and T. P. Devereaux, Phys. Rev. X **6**, 021020 (2016).
[52] M. Minola, Y. Lu, Y. Y. Peng, G. Dellea, H. Gretarsson, M. W. Haverkort, Y. Ding, X. Sun, X. J. Zhou, D. C. Peets, L. Chauviere, P. Dosanjh, D. Bonn, R. Liang, A. Damascelli, M. Dantz, X. Lu, T. Schmitt, L. Braicovich, G. Ghiringhelli, B. Keimer, and M. Le Tacon, Phys. Rev. Lett. **119**, 097001 (2017).
[53] Y. Lu and M. W. Haverkort, Phys. Rev. Lett. **119**, 256401 (2017).
[54] L. Braicovich, J. van den Brink, V. Bisogni, M. M. Sala, L. J. P. Ament, N. B. Brookes, G. M. De Luca, M. Salluzzo, T. Schmitt, V. N. Strocov, and G. Ghiringhelli, Phys. Rev. Lett. **104**, 077002 (2010).
[55] M. W. Haverkort, M. Zwierzycki, and O. K. Andersen, Phys. Rev. B **85**, 165113 (2012).
[56] N. Majlis, *The Quantum Theory of Magnetism* (World Scientific, Singapore, 2000).
[57] R. D. Cowan, *The Theory of Atomic Structure and Spectra* (University of California Press, Berkeley, 1981).